

# Constrained Gaussian Random Fields with Continuous Linear Boundary Restrictions for Physics-informed Modeling of States

Yue Ma\*

Department of Statistics, The Ohio State University

Oksana A. Chkrebtii

Department of Statistics, The Ohio State University

Stephen R. Niezgoda

Department of Materials Science and Engineering, The Ohio State University

December 5, 2025

## Abstract

Boundary constraints in physical, environmental and engineering models restrict smooth states such as temperature to follow known physical laws at the edges of their spatio-temporal domain. Examples include fixed-state or fixed-derivative (insulated) boundary conditions, and constraints that relate the state and the derivatives, such as in models of heat transfer. Despite their flexibility as prior models over system states, Gaussian random fields do not in general enable exact enforcement of such constraints. This work develops a new general framework for constructing linearly boundary-constrained Gaussian random fields from unconstrained Gaussian random fields over multi-dimensional, convex domains. This new class of models provides flexible priors for modeling smooth states with known physical mechanisms acting at the domain boundaries. Simulation studies illustrate how such physics-informed probability models yield improved predictive performance and more realistic uncertainty quantification in applications including probabilistic numerics, data-driven discovery of dynamical systems, and boundary-constrained state estimation, as compared to unconstrained alternatives.

*Keywords:* Gaussian processes; spatial constraints; surrogate models; partial differential equations; probabilistic numerics

---

\*The authors would like to acknowledge support from the U.S. National Science Foundation Engineering Research Center for Hybrid Autonomous Manufacturing Moving from Evolution to Revolution (ERC-HAMMER) under Award Number EEC-2133630.

# 1 Introduction

In the physical, environmental, and engineering sciences, where modeling smooth states is of interest, there is often complete information about the states at the domain boundaries. For example, when modeling temperature, insulation at the boundary leads to fixed-derivative constraints, while heat transfer results in constraints on linear combinations of the state and its derivatives (e.g., [Hahn & Özisik 2012](#), [Bird et al. 2006](#)). Another example from materials science consists of modeling the displacement field along a material sample to study its response to pulling forces. A typical experimental set-up is illustrated in the left-hand panel of [Figure 1](#) and shows that a statistical model should account for the known uniform motion at the upper boundary and zero displacement at the lower boundary of the material sample (e.g., [Hosford 2005](#), [Arfken et al. 2012](#)). Beyond physical restrictions, in the setting of computer model calibration, a fixed-state constraint over the response surface results when a complex mathematical model has an analytical solution for specific parameter combinations ([Vernon et al. 2019](#), [Ye & Tan 2022](#)). Consequently, a prior model that enforces these constraints results in a more accurate surrogate model. Another important application is in constructing scalable approaches for fitting nonstationary models to large datasets, where some approaches (e.g., [Gramacy & Apley 2015](#), [Huang et al. 2025](#)) fit local models independently over disjoint domain partitions, necessitating fixed-state constraints at partition boundaries to ensure continuity of the underlying smooth states. In all these settings, flexible boundary-constrained priors are needed for improved predictive performance and uncertainty quantification given limited measurements.

Existing approaches for constructing Gaussian random fields (GRFs) with boundary constraints are limited to specific covariance structures, hyperparameter choices, and constraint types on 1-dimensional intervals or 2-dimensional rectangular domains ([Ding et al. 2019](#), [Chkrebtii 2013](#), [Gasbarra et al. 2007](#), [Ye & Tan 2022](#), [Tan 2018](#), [Dalton et al. 2024](#), [Vernon](#)

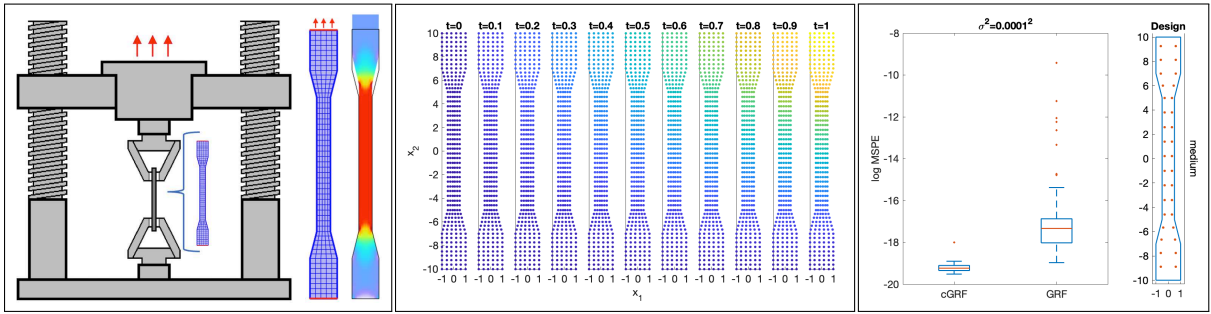


Figure 1: Left panel: illustration of tensile strength test and corresponding constraints at two parallel boundaries (red horizontal lines). Center panel: displacement over time from left to right; lighter colors represent greater displacement. Right panel: box plots comparing  $\log MSPE$  under a constrained vs unconstrained GRF prior on the displacement field.

et al. 2019). When extending beyond these cases, a common strategy is to rely on approximations, giving up either deriving analytical expressions for mean and covariance functions, or enforcing continuous constraints at multi-dimensional boundaries (Solin & Kok 2019, Wang & Berger 2016). However, as will be illustrated in Section 4, it is often desirable to maintain the flexibility of constrained GRF priors without relying on approximations. We propose a new framework to construct GRFs with continuous linear boundary restrictions over multi-dimensional, convex domains (as illustrated in Figure 2) by transforming appropriately smooth unconstrained GRFs. Expressions for the mean and covariance function of these restricted models are available in closed form, facilitating computation.

## 1.1 Relation to existing work

Recent work on enforcing boundary constraints takes a spectral approach by relating the GRF covariance operator to the elliptic operators. Solin & Kok (2019) first introduced a new covariance structure  $k^{\partial\mathcal{D}}(x, x') = \sum_j s(\lambda_j^{-1/2}) \psi_j(x) \psi_j(x')$ , where  $s$  is the spectral density of a stationary, isotropic covariance function, and  $\lambda_j$  and  $\psi_j$  for  $j = 1, 2, \dots$  are eigenvalues and eigenfunctions of the Laplace operator  $\Delta$ , respectively. For a domain  $\mathcal{D}$  with boundary  $\partial\mathcal{D}$ ,  $\lambda_j$  and  $\psi_j$  are obtained by solving the eigenvalue problem  $-\Delta\psi_j(x) = \lambda_j\psi_j(x)$  for  $x \in \mathcal{D}$ , and  $\psi_j(x) = 0$  for  $x \in \partial\mathcal{D}$ . Since  $\psi_j$  approach 0 as  $x$  approaches  $\partial\mathcal{D}$ , the

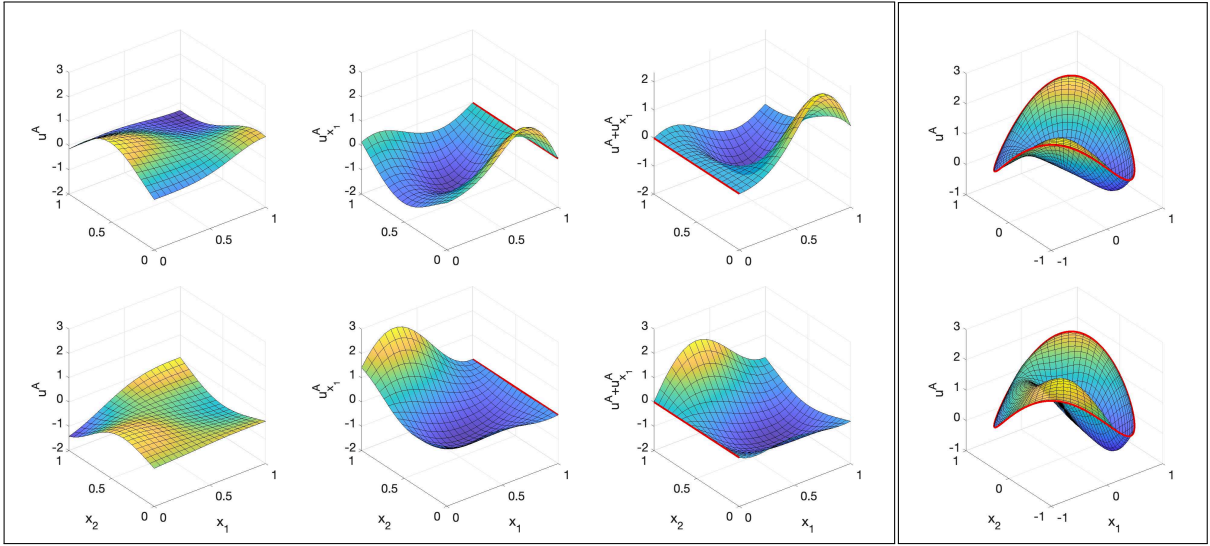


Figure 2: Pairs of realizations (top and bottom rows) from the marginal cGRF model with boundary constraints shown in red. Left panel from left to right: state, first derivative, and linear combination of state and derivative over a rectangular domain. Right panel: state over a disk-shaped domain.

new class of covariance functions  $k^{\partial\mathcal{D}}$  define GRFs with fixed-state boundary constraints. However, as pointed out by [Solin & Kok \(2019\)](#) and [Gulian et al. \(2022\)](#), except for fixed-state boundary constraints on rectangular or spherical domains, or certain types of mixed boundary constraints on rectangular domains, the eigenvalues and eigenfunctions typically need to be approximated via discretization. Although appropriate in their specific context, the approximation means that boundary enforcement for the desired domains is no longer exact, resulting in less realistic modeling. Furthermore, the spectral approach is incompatible with nonstationary, anisotropic base covariance functions, and constraints on segments of the boundary. See [Padilla-Segarra et al. \(2025\)](#) for another spectral construction that applies a numerical method for approximating constrained covariances.

Another existing approach is to directly derive analytical expressions for GRF covariance functions to attain fixed-endpoint constraints on a 1-dimensional domain at one or both endpoints by repeatedly integrating an initial stationary covariance. Such expressions, derived from the squared exponential and uniform covariances, and the Matérn covariance

were obtained in [Chkrebtii \(2013\)](#) and [Ye & Tan \(2022\)](#), respectively. In addition to being restricted to cases where such analytical integrals are available, extensions to multi-dimensional domains are restricted to a product-form covariance specification, making the approach limited in practice. Adopting a different strategy, [Ding et al. \(2019\)](#) provide a closed-form expression for a state-constrained covariance derived from a Matérn covariance with smoothness hyperparameter 0.5 called *BdryMatérn*.

Another direct approach to covariance specification, introduced in [Tan \(2018\)](#), formulated the covariance as  $k^{\partial\mathcal{D}}(x, x') = \phi(x)\phi(x')\rho(x, x')$ , using a correlation function  $\rho$ , and an approximate distance function (ADF)  $\phi$  that approaches 0 as  $x$  approaches the boundary, to enforce fixed-state boundary constraints. [Dalton et al. \(2024\)](#) extended this approach and provided recipes for enforcing certain types of mixed boundary constraints by further restricting the ADF, referred to as normalization. They draw connections between directly specifying the covariances and transforming existing GRFs on a case-by-case basis. In practice, curved domain boundaries are approximated using a piecewise linear function, and each piece is assigned an individual ADF, all of which are joined into a global ADF. Besides introducing approximation, as noted by [Dalton et al. \(2024\)](#), the normalization of the global ADF, a necessary condition for enforcing fixed-derivative constraints, fails at the segment joints. Furthermore, from a modeling perspective, it is important to directly address smoothness.

[Gasbarra et al. \(2007\)](#) generalize Brownian bridges to *Gaussian bridges*, illustrated in the top left panel of Figure 3. These are Gaussian processes on 1-dimensional intervals that are restricted at both endpoints through conditioning on the boundary values. [Gasbarra et al. \(2007\)](#) show that this conditioned measure is well defined. However, this approach does not straightforwardly generalize to higher-dimensional domains. Indeed, a related proposal by [Vernon et al. \(2019\)](#) for imposing continuous constraints across edges of a rectangular

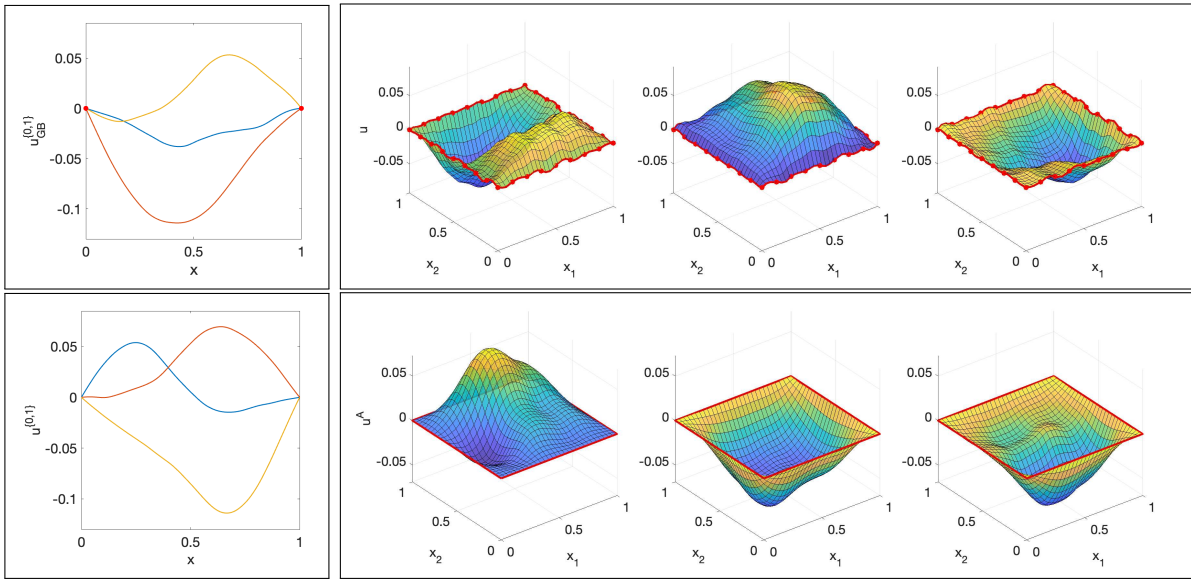


Figure 3: Top left panel: three samples from a Gaussian bridge from  $(0,0)$  to  $(1,0)$ ; Top right panel: three samples from a point-wise conditioned GRF; Bottom panels: three samples from cGRFs on 1- and 2-dimensional spatial domains with continuously enforced boundary constraints. Red lines and points represent the state and synthetic observations at the boundary, respectively.

domain by conditioning on a restriction over an uncountable set lacks an analogous justification. Alternatively, [Wang & Berger \(2016\)](#) suggest conditioning a GRF on a large (but finite) set of synthetic error-free observations to enforce constraints across segments of spatial domains. However, although GRFs can be quite flexible in interpolating those observations, the required covariance matrix inversion quickly becomes computationally prohibitive. More importantly, this method cannot exactly enforce continuous, infinite-dimensional boundary constraints, as illustrated in the top row of [Figure 3](#).

In contrast to existing methods that either define constrained covariance structures in limited settings or rely on approximations of domains or constraints, our approach directly transforms an existing GRF into one that exactly satisfies the desired boundary constraints. We explicitly account for smoothness and provide sufficient conditions on the transformation to enforce linear boundary constraints on multi-dimensional convex domains.

## 1.2 Contributions

Our approach for constructing linearly boundary-constrained GRFs is fundamentally different from the existing methods summarized in Section 1.1, although some of their resulting covariance structures naturally arise from our approach, as shown in the supplement. The first contribution in Section 3 is a definition of a constrained random field satisfying continuous linear boundary restrictions, which we refer to interchangeably as a *boundary-constrained* or *linearly-constrained* random field. This definition leads to our main contribution, which is a representation-based framework to construct constrained GRFs by transforming suitably smooth unconstrained base GRFs. We call this class of models *cGRF* and our approach the *cGRF framework*. Our constructive approach for defining cGRFs retains some properties of the base GRF, such as smoothness, while enforcing constraints at the boundaries. Crucially, constructing cGRFs does not require approximation, and the corresponding mean and covariance functions can be obtained in closed form. The framework is compatible with a wide range of linear boundary constraints and convex regular domains, resulting in flexible functional priors for a variety of applications. As examples, we employ cGRFs as prior models of system states on problems in probabilistic numerics (Cockayne et al. 2019, Chkrebtii et al. 2016) and data-driven discovery of dynamical systems (North et al. 2023, 2025, Chen et al. 2020). In these cases, enforcing known constraints on the system states leads to more realistic models, which translates into improved estimation accuracy. Lastly, we apply our approach to the problem of boundary-constrained inference on the displacement field over a material sample from discrete tensile test measurements, which is an important step for ensuring that materials used in industrial application meet safety and performance standards.

## 2 Background

We briefly review Gaussian random field (GRF) models and their use as priors over unknown states for Bayesian function estimation. This is followed by a review of a class of GRFs on a 1-dimensional domain called *Gaussian bridges* (Gasbarra et al. 2007), which impose fixed-state constraints at the endpoints. We note that our proposed framework is both fundamentally different and more general than the Gaussian bridge.

GRFs are probability models of smooth states over a spatio-temporal domain  $\mathcal{D}$ , which are fully specified by their mean  $m(x) = \mathbb{E}[u(x)]$  and covariance function  $k(x, x') = \mathbb{E}[(u(x) - m(x))(u(x') - m(x'))]$  for  $x, x' \in \mathcal{D}$ . We say that  $\{u(x), x \in \mathcal{D}\}$  is a GRF, denoted by  $u(x) \sim \text{GRF}(m(x), k(x, x'))$ , if any finite collection  $u = (u(x_1), \dots, u(x_n))$  follows a multivariate normal distribution  $\mathcal{N}(\mu, K)$  with the mean vector and covariance matrix having entries  $\mu_i = m(x_i)$  and  $K_{ij} = k(x_i, x_j)$ , respectively, for  $i, j = 1, \dots, n$ . The covariance function controls the degree of dependence in the state at nearby locations on the domain. An example of a flexible stationary covariance structure is the Matérn function

$$k(x, x') = \alpha^{-1} \frac{1}{\Gamma(\nu) 2^{\nu-1}} \left( \frac{\sqrt{2\nu} \|x - x'\|}{\lambda} \right)^\nu K_\nu \left( \frac{\sqrt{2\nu} \|x - x'\|}{\lambda} \right), \quad \alpha, \lambda, \nu > 0,$$

where  $K_\nu$  is the modified Bessel function of the second kind. A special case called the squared exponential covariance is obtained in the limit as  $\nu \rightarrow \infty$ . GRFs with squared exponential covariance are infinitely sample-path differentiable, and GRFs with Matérn covariance are  $\lceil \nu \rceil - 1$  times sample-path differentiable (Paciorek 2003, Wang et al. 2021). The hyperparameters  $\alpha, \lambda$ , and  $\nu$  determine the prior variance, length-scale, and degree of smoothness, respectively.

An important property of GRFs which enables our framework is that they retain Gaussianity under linear operations  $\mathcal{L} : \mathcal{H} \rightarrow \mathcal{H}'$ , including integration, differentiation, and



composition. Indeed, if  $u$  is a GRF with mean  $m$  and covariance  $k$  such that  $\mathcal{L}u$  exists, then  $\mathcal{L}u$  is also a GRF with mean  $\mathcal{L}m$  and covariance  $\mathcal{L}k\mathcal{L}^*$ , where  $\mathcal{L}^*$  denotes the adjoint of  $\mathcal{L}$ . For example, if  $\mathcal{L}$  is the differential operator, and  $m$  and  $k$  are such that  $u$  is sample-path differentiable, then the GRF  $\mathcal{L}u$  is well defined. As another example, the composition of a GRF with a deterministic function  $f : \mathcal{D} \rightarrow \mathcal{D}$  remains a GRF.

Pointwise boundary enforcement is possible by conditioning a prior GRF measure on error-free measurements  $y = \mathcal{L}u$  at finitely many boundary points  $x \in \partial\mathcal{D}$ . If  $u$  is a GRF prior with mean  $m_0$  and covariance  $k_0$ , the posterior measure is likewise a GRF with mean and covariance,

$$\begin{aligned} m(x) &= m_0(x) + k_0\mathcal{L}^*(x, X) [\mathcal{L}k_0\mathcal{L}^*(X, X)]^{-1} (y - \mathcal{L}m_0(X)), \\ k(x, x') &= k_0(x, x') - k_0\mathcal{L}^*(x, X) [\mathcal{L}k_0\mathcal{L}^*(X, X)]^{-1} \mathcal{L}k_0(X, x'). \end{aligned} \tag{1}$$

Here  $k(X, X')$  for a covariance  $k$  denotes an  $n \times m$  matrix with  $(i, j)$ th element  $k(x_i, x_j)$  where  $X = (x_1, \dots, x_n)$  and  $X' = (x'_1, \dots, x'_m)$ . Similar updates are available for conditioning on measurements of the state across the domain with additive Gaussian error. These closed-form updates make GRFs natural candidates for active learning algorithms for sequential experimental design (Santner et al. 2003, Chen et al. 2020) and smoothing problems in spatial statistics (Stein 1999, Banerjee et al. 2004, Schabenberger & Gotway 2004).

The *Gaussian bridge* (Gasbarra et al. 2007) is one example on a 1-dimensional domain, where a Gaussian process (GP) is conditioned on two synthetic measurements at the endpoints, as illustrated in the top left panel of Figure 3. The Gaussian bridge defines constrained GPs through a representation, from which corresponding mean and covariance functions may be computed (we will show that the Gaussian bridge representation arises as a special case of the cGRF for a 1-dimensional domain). Consider the interval  $[0, T]$ , two scalars  $\xi$  and  $\theta$ , and a Gaussian process  $u_{GB}^{\{0\}}$  with  $u_{GB}^{\{0\}}(0) = \xi$ . Gasbarra et al. (2007)

provides the following proposition. Let  $u_{GB}^{\{0\}}$  be a Gaussian process with mean function  $m_{GB}^{\{0\}}$  and covariance function  $k_{GB}^{\{0\}}$ . Then the Gaussian bridge  $u_{GB}^{\{0,T\}}$  from  $(0, \xi)$  to  $(T, \theta)$  admits a representation  $u_{GB}^{\{0,T\}}(x) = u_{GB}^{\{0\}}(x) + k_{GB}^{\{0\}}(T, x) k_{GB}^{\{0\}}(T, T)^{-1} (\theta - u_{GB}^{\{0\}}(T))$  with mean and covariance functions

$$\begin{aligned} m_{GB}^{\{0,T\}}(x) &= m_{GB}^{\{0\}}(x) + k_{GB}^{\{0\}}(T, x) k_{GB}^{\{0\}}(T, T)^{-1} (\theta - m_{GB}^{\{0\}}(T)), \\ k_{GB}^{\{0,T\}}(x, x') &= k_{GB}^{\{0\}}(x, x') - k_{GB}^{\{0\}}(T, x) k_{GB}^{\{0\}}(T, T)^{-1} k_{GB}^{\{0\}}(T, x'). \end{aligned}$$

Generalizations to higher-dimensional domains are not available, as they require proving that measures conditioned on states over a continuous boundary are well defined. We instead adopt a constructive approach, based on linear transformation of a suitably smooth base GRF, which constrains the states without explicitly conditioning.

### 3 Methodology

We begin by defining what we mean for a random field to be *linearly-constrained* over a segment of the domain boundary. Throughout the presentation, we define random fields on a probability space  $(\Omega, \mathcal{F}, P)$  over a spatial domain  $\mathcal{D} \subset \mathbb{R}^d$  with boundary  $\partial\mathcal{D}$ , taking values in a Hilbert space  $\mathcal{H}$ . Moreover, we write that two random fields equal to each other when they equal in law. When we say that a random field is sample-path continuous or sample-path differentiable, we mean that there exists a modification that is sample-path continuous or sample-path differentiable (see, for e.g., [Seeger 2004](#), [Paciorek 2003](#), [Wang et al. 2021](#)).

**Definition 1** *Let  $\mathcal{L} : \mathcal{H} \rightarrow \mathcal{H}'$  be a linear operator,  $g : \mathcal{D} \rightarrow \mathbb{R}$  be a target function, and  $A \subset \partial\mathcal{D}$  be a segment of the boundary. We say that a random field  $u^A : \mathcal{D} \times \Omega \rightarrow \mathbb{R}$  is linearly-constrained if  $\mathcal{L}u^A$  is sample-path continuous and  $\mathcal{L}u^A(x)$  equals  $g(x)$  almost surely for all  $x \in A$ .*

While Definition 1 includes any sample-path continuous random field that satisfies the boundary constraint with probability one, this paper focuses on the Gaussian case in particular. We construct a linearly-constrained Gaussian random field, termed *cGRF*, as

$$u^A \sim \text{GRF}(m^A, k^A) := \text{cGRF}(\mathcal{L}, g, A, m_0, k_0), \quad (2)$$

by transforming a base unconstrained GRF  $u \sim \text{GRF}(m_0, k_0)$  into a GRF with mean  $m^A$  and covariance  $k^A$ .

In the remainder of Section 3, we develop representations of cGRF models of states under various linear boundary constraints on multi-dimensional convex domains. Section 3.1 introduces the *projection* and *weight* functions used to construct cGRFs. Section 3.2 presents our framework for constructing cGRF representations along with closed-form expressions for their mean and covariance functions. Section 3.3 provides a recipe for constructing weight functions.

### 3.1 Preliminaries for constructing cGRFs

In this section, we discuss different types of linear boundary constraints and introduce the projection and weight functions used in the representations in Section 3.2. For simplicity in this section we take  $g = 0$ , and consider more general choices in Section 3.2. To build an intuitive understanding of the approach, we begin by constructing a cGRF on a 1-dimensional interval with a single endpoint constraint.

**Example 1** *We wish to construct a GRF constrained to  $g = 0$  at the left endpoint  $A = \{0\}$  on the 1-dimensional domain  $\mathcal{D} = [0, 1]$ , denoted by  $u^{\{0\}} \sim \text{cGRF}(\mathcal{I}, 0, \{0\}, m_0, k_0)$ , where  $\mathcal{I}$  is the identity operator, and  $m_0$  and  $k_0$  are the mean and covariance of a base GRF  $u$ . Consider the transformation  $u^{\{0\}}(x) = u(x) - u(0)$  of  $u$ . It is clear that  $u^{\{0\}}(x) = 0$  almost*

surely at  $x = 0$ , and  $u^{\{0\}}$  is as smooth as  $u$  across the domain. Its mean and covariance functions are  $m^{\{0\}}(x) = m_0(x) - m_0(0)$ , and  $k^{\{0\}}(x, x') = k_0(x, x') - k_0(x, 0) - k_0(0, x') + k_0(0, 0)$ , respectively. The supplement shows that  $k^{\{0\}}$  is the covariance derived directly in [Chkrebtii \(2013\)](#) and [Ye & Tan \(2022\)](#).

Section [3.2](#) describes a framework for enforcing more general constraints over multi-dimensional domains. For this, we next introduce the projection and weight functions  $f$  and  $w$ .

### 3.1.1 Multi-dimensional convex domains

Constraints on multi-dimensional domains are typically defined over continuous boundary segments, such as the sides of a rectangular domain or segments of the circular boundary of a disk-shaped domain. Recall that  $A \subset \partial\mathcal{D}$  denotes the segment or set of segments where one wishes to enforce constraints. Below we use examples to introduce the projection function  $f$  and relate it to  $A$ . Implementation details for cGRFs on the unit disk and unit triangle are provided in the the supplement.

**Example 2** For the unit square domain  $\mathcal{D} = [0, 1]^2$ , three examples of boundary segments  $A$  are the left side  $\{(x_1, x_2) \in \partial\mathcal{D} \mid x_1 = 0\}$ , the two parallel sides  $\{(x_1, x_2) \in \partial\mathcal{D} \mid x_1 = 0 \text{ or } x_1 = 1\}$ , and the two adjacent sides  $\{(x_1, x_2) \in \partial\mathcal{D} \mid x_1 = 0 \text{ or } x_2 = 0\}$ , illustrated in red in the first three panels of [Figure 4](#). For the unit disk domain  $\mathcal{D} = \{(x_1, x_2) \in \mathbb{R}^2 \mid x_1^2 + x_2^2 \leq 1\}$ , two examples of boundary segments  $A$  are the half circle  $\{(x_1, x_2) \in \partial\mathcal{D} \mid x_1 = -(1 - x_2^2)^{1/2}\}$ , and the full circle  $\{(x_1, x_2) \in \partial\mathcal{D}\}$ , illustrated by the last two panels of [Figure 4](#).

For a given boundary segment  $A$ , the cGRF construction requires a continuous function  $f : \mathcal{D} \rightarrow A \subset \mathcal{D}$  mapping interior points in  $\mathcal{D}$  onto  $A$  and mapping points in  $A$  onto themselves, i.e.,  $f(x) = x$  when  $x \in A$ . Notice that  $u^{\{0\}}(x)$  in [Example 1](#) can be equivalently

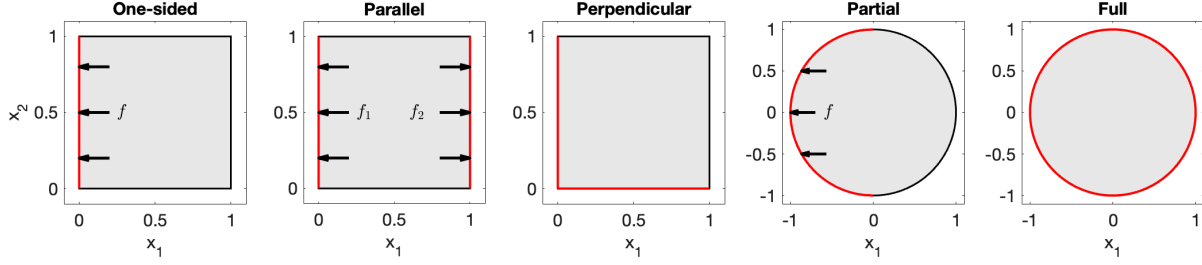


Figure 4: Five examples of boundary segments  $A$  (red lines) and the corresponding projection function(s) in three cases (black arrows).

represented as  $u(x) - u \circ f(x)$  with  $f(x) = 0$ , for all  $x \in [0, 1]$ .

**Example 2 (Continued).** For the unit square domain, we construct a cGRF constrained to  $g = 0$  at the left side  $A = \{(x_1, x_2) \in \partial\mathcal{D} \mid x_1 = 0\}$  via the representation  $u^A(x_1, x_2) = u(x_1, x_2) - u \circ f(x_1, x_2)$  with  $f(x_1, x_2) = (0, x_2)$ , for all  $(x_1, x_2) \in \mathcal{D}$ . Similarly, for the unit disk domain, a cGRF constrained to  $g = 0$  at the half circle  $A = \{(x_1, x_2) \in \partial\mathcal{D} \mid x_1 = -(1 - x_2^2)^{1/2}\}$  is obtained as  $u^A(x_1, x_2) = u(x_1, x_2) - u \circ f(x_1, x_2)$  with  $f(x_1, x_2) = (-(1 - x_2^2)^{1/2}, x_2)$ , for all  $(x_1, x_2) \in \mathcal{D}$ . In both settings,  $f$  is the projection of interior points  $x$  to the boundary segment  $A$ , along the direction  $(-1, 0)$  (first and fourth panels of Figure 4).

**Example 3 (Relaxation of convexity)** We restrict our discussion to convex domains to avoid violating the continuity of the projection function  $f$ . Essentially, on a non-convex domain, two spatial coordinates close to each other can be projected to two coordinates far away from each other on the boundary. For instance, the continuous projection function on the disk-shaped domain, illustrated by the fourth panel in Figure 4, fails to be continuous for a ring-shaped (annular) domain. This restriction on the domain may be relaxed, either by exploring alternative options for  $f$ , or if constraints are enforced only on a segment of the boundary. The application on tensile testing in Section 4 demonstrates constraining the state at parallel sides of a dog-bone-shaped domain.

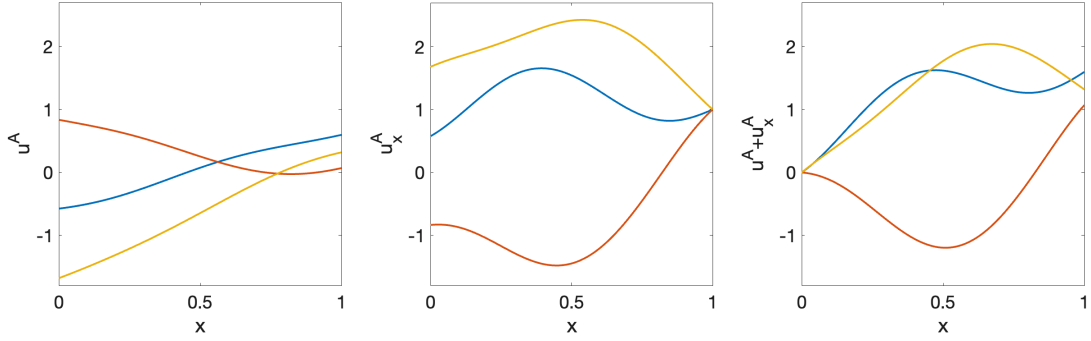


Figure 5: Marginal cGRF samples (blue, yellow, and orange lines) over state  $u^A$ , first derivative  $u_x^A$ , and  $u^A + u_x^A$  (from left to right). The first derivative is constrained to 1 at the right endpoint; while  $u^A + u_x^A$  is constrained to 0 at the left endpoint.

### 3.1.2 Constraining linear transformations of the states

We introduce the weight function,  $w : \mathcal{D} \rightarrow \mathbb{R}$ , to achieve two other generalizations. The first is to impose a constraint involving a linear transformation  $\mathcal{L}$  of the state. In this case,  $w$  activates the constraint only when  $\mathcal{L}$  is applied.

**Example 1 (Continued).** Consider the first-order differential operator  $\mathcal{L} = \partial_x$ . Returning to the 1-dimensional domain, we wish to construct  $u^{\{0\}} \sim \text{cGRF}(\partial_x, 0, \{0\}, m_0, k_0)$  to satisfy the constraint  $\partial_x u^{\{0\}}(x) = 0$  at  $x = 0$ . One such representation is  $u^{\{0\}}(x) = u(x) - w(x)(\partial_x u \circ f(x))$ , where  $f(x) = 0$ , and  $w(x) = x$  for all  $x \in [0, 1]$ . Notice that  $\partial_x u^{\{0\}}(x) = \partial_x u(x) - \partial_x u(0)$ , so that  $\partial_x u^{\{0\}}$  is constrained to  $g = 0$  at  $A = \{0\}$ . The center panel in Figure 5 shows a cGRF with fixed-derivative boundary constraint at the right endpoint. To simultaneously enforce the constraint at the left endpoint, as shown in the right panel, refer to the discussion in Section 3.3. The supplement shows that  $u^{\{0\}}$  is related to Eq. (27) in Dalton et al. (2024) for a fixed-derivative boundary constraint.

Another generalization consists of imposing different boundary constraints across disjoint boundary segments. Consider a set of  $n$  weight functions,  $w = \{w_i \mid i = 1, \dots, n\}$ , where  $n$  is the number of constraints.  $w$  activates the corresponding constraints as  $x$  approaches different segments of the boundary. See Section 3.3 for a recipe for constructing  $w$ .

This generalization is also convenient for relaxing the restriction on the projection function  $f$  when a single projection for the entire set of boundary segments  $A$  is unavailable, by treating the constraint on  $A$  as multiple constraints of the same type defined on disjoint segments of  $A$ .

**Example 2 (Continued).** *For the two-sided parallel boundary constraint on the unit square domain, the function  $f$  cannot simultaneously map  $x \in \mathcal{D}$  to the parallel sides  $A$ , while ensuring that  $f(x) = x$  at  $A$ . Hence, we partition  $A$  into  $A_1 = \{(x_1, x_2) \in \partial\mathcal{D} \mid x_1 = 0\}$  and  $A_2 = \{(x_1, x_2) \in \partial\mathcal{D} \mid x_1 = 1\}$ , and construct  $u^{\{A_1, A_2\}}(x_1, x_2) = u(x_1, x_2) - w_1(x_1, x_2)(u \circ f_1(x_1, x_2)) - w_2(x_1, x_2)(u \circ f_2(x_1, x_2))$ , where  $f_1(x_1, x_2) = (0, x_2)$ ,  $f_2(x_1, x_2) = (1, x_2)$ ,  $w_1(x_1, x_2) = 1 - x_1$ , and  $w_2(x_1, x_2) = x_1$ , for  $(x_1, x_2) \in \mathcal{D}$  (see the second plot of Figure 4 for illustration of  $f_1, f_2$ ). Notice that  $\{w_1, w_2\}$  approaches  $\{0, 1\}$  and  $\{1, 0\}$ , as  $x_1$  approaches 0 and 1, respectively, and that as a result,  $u^{\{A_1, A_2\}}$  is constrained to 0 across  $A$ .*

## 3.2 A general cGRF representation

This section formally introduces the cGRF framework. Theorem 1 provides sufficient conditions on the base GRF  $u$ , and the custom projection and weight functions introduced in Section 3.1, for the constrained GRF  $u^A$  to satisfy  $\mathcal{L}_i u^A(x) = g_i(x)$  for all  $x \in A_i$ ,  $i = 1, \dots, n$ . Explicit expressions for the mean and covariance functions of  $u^A$  are also provided.

**Theorem 1** *For  $i = 1, \dots, n$ , let  $\mathcal{L}_i : \mathcal{H} \rightarrow \mathcal{H}'_i \subset \mathcal{C}(\mathcal{D})$  be a linear operator, let  $g_i : \mathcal{D} \rightarrow \mathbb{R}$  be a target function, let  $A_i \subset \partial\mathcal{D}$  be a boundary segment such that there exists a continuous projection function  $f_i : \mathcal{D} \rightarrow A_i$  satisfying  $f_i(x) = x$  for all  $x \in A_i$ , and let  $w_i : \mathcal{D} \rightarrow \mathbb{R}$  be a weight function. Let  $u : \mathcal{D} \times \Omega \rightarrow \mathbb{R}$  be a Gaussian random field such that  $u(\cdot, \omega) \in \mathcal{H}$*

for  $P$ -almost all  $\omega \in \Omega$ . Furthermore, assume that for  $i, j = 1, \dots, n$ ,

$$w_j(\cdot) (g_j \circ f_j(\cdot) - \mathcal{L}_j u \circ f_j(\cdot, \omega)) \in \mathcal{H} \quad (3)$$

for  $P$ -almost all  $\omega \in \Omega$ , and for all  $x \in A_i$ ,

$$\mathcal{L}_i [w_j(x) (g_j \circ f_j(x) - \mathcal{L}_j u \circ f_j(x))] = \begin{cases} g_j \circ f_j(x) - \mathcal{L}_i u \circ f_j(x), & j = i \\ 0, & j \neq i \end{cases} \quad (4)$$

then a linearly-constrained Gaussian random field  $u^A$  can be constructed as

$$u^A(x) = u(x) + \sum_{j=1}^n w_j(x) (g_j \circ f_j(x) - \mathcal{L}_j u \circ f_j(x)). \quad (5)$$

**Proof 1** *The proof is provided in the supplement.*

We denote the resulting linearly-constrained cGRF model of the state satisfying the set of given linear boundary constraints by  $u^A \sim cGRF(\mathcal{L}, g, A, m_0, k_0)$ , where  $\mathcal{L} = \{\mathcal{L}_i \mid i = 1, \dots, n\}$ ,  $g = \{g_i \mid i = 1, \dots, n\}$ , and  $A = \{A_i \mid i = 1, \dots, n\}$ . As before,  $m_0$  and  $k_0$  are the mean and covariance of the base GRF  $u$ . Note that the representation (5) for a given set of linear boundary constraints is not unique since it is based on the choice of  $f$  and  $w$ . Examples in Section 3.1 are special cases of (5).

An important advantage of Theorem 1 is that it does not require establishing the existence of probability measures conditioned on restrictions over a continuous set, such as constraints over multi-dimensional domain boundaries (see, e.g., Stuart 2010, Cockayne et al. 2019, for a discussion of challenges in proving the existence of such conditioned measures). Instead, our constructive approach uses well-known properties of linear transformations of GRFs to transform a base GRF into one that satisfies the desired constraints. Our ap-



proach also assumes appropriate choices of  $k_0, m_0, w_j, g_j$  and  $f_j$  such that  $u(\cdot, \omega) \in \mathcal{H}$  and  $w_j(\cdot) (g_j \circ f_j(\cdot) - \mathcal{L}_j u \circ f_j(\cdot, \omega)) \in \mathcal{H}$  for  $j = 1, \dots, n$ . For example, Matérn covariances are convenient candidates for  $k_0$  when  $\mathcal{H} \subset \mathcal{C}^\beta(\mathcal{D})$ , for  $\beta \in \mathbb{N}_0^d$  and  $\mathcal{L}$  involves linear partial differential operators. In addition, we also need to ensure that  $m_0, w_j, g_j, f_j \in \mathcal{H} \subset \mathcal{C}^\beta(\mathcal{D})$  for  $j = 1, \dots, n$  (see, e.g., [Wang et al. 2021](#)). Candidates for  $\mathcal{H}$  and  $\mathcal{H}'_i$  are Sobolev spaces with  $p = 2$ . Candidates for  $f_j$  are continuous functions projecting interior points to the boundary and boundary points to themselves, along one of the signed coordinate directions  $(\pm 1, 0, \dots, 0), (0, \pm 1, 0, \dots, 0), (0, \dots, 0, \pm 1)$ . If necessary, we further partition  $A$  to accommodate such choices of  $f_j$ , as in Example 2. Lemma 1 provides the mean and covariance of the cGRF  $u^A$  constructed in Theorem 1.

**Lemma 1** *The mean and covariance function of  $u^A \sim \text{cGRF}(\mathcal{L}, g, A, m_0, k_0)$  are*

$$\begin{aligned} m^A(x) &= m_0(x) + \sum_{j=1}^n w_j(x) (g_j(f_j(x)) - \mathcal{L}_j m_0(f_j(x))), \\ k^A(x, x') &= k_0(x, x') - \sum_{j'=1}^n w_{j'}(x') k_0 \mathcal{L}_{j'}^*(x, f_{j'}(x')) - \sum_{j=1}^n w_j(x) \mathcal{L}_j k_0(f_j(x), x') \\ &\quad + \sum_{j=1}^n \sum_{j'=1}^n w_j(x) w_{j'}(x') \mathcal{L}_j k_0 \mathcal{L}_{j'}^*(f_j(x), f_{j'}(x')). \end{aligned}$$

**Proof 2** *The proof follows directly from Theorem 1 and the properties of GRFs.*

Figures 2, 5, and 6 illustrate samples from various cGRFs. Another interesting consequence of Theorem 1 is illustrated in the bottom row of Figure 6. For a rectangular domain, the constrained covariance  $k^A(x, x') = k_1(x_1, x'_1) k_2^A(x_2, x'_2)$  inherits the product covariance structure from the base covariance  $k_0(x, x') = k_1(x_1, x'_1) k_2(x_2, x'_2)$ , as shown in the supplement for the case where  $k_1$  and  $k_2$  are periodic and Matérn covariances. As a result, the three samples from the resulting cGRF shown in the bottom row of Figure 6 satisfy periodic and fixed-state constraints in dimensions  $x_1$  and  $x_2$ , respectively. In general, however, the cGRF framework accommodates any form of multi-dimensional base covariance  $k_0$  under

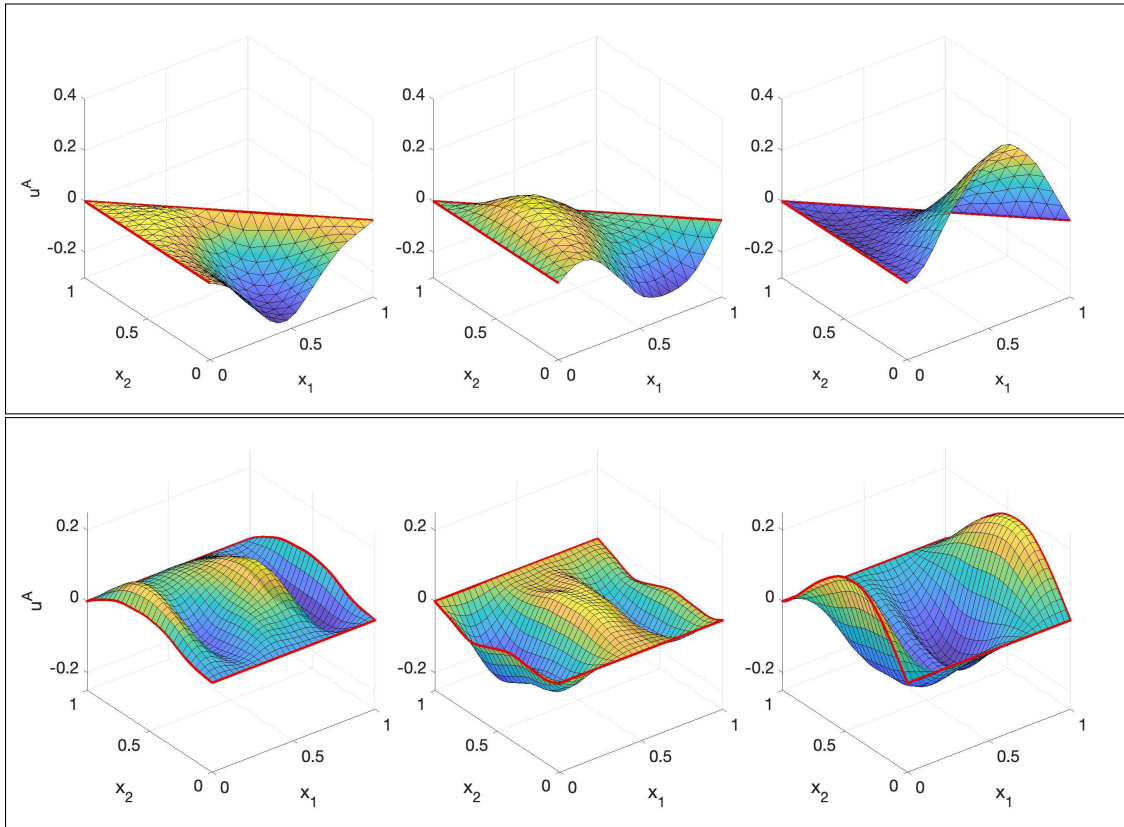


Figure 6: Three samples from a cGRF on the triangular domain (top row) and the unit square domain (bottom row; base covariances have product structure with periodic and Matérn components, respectively). Red solid lines indicate boundary constraints.

the conditions in Theorem 1.

### 3.3 Constructing weight functions

Next, we provide some guidance on how to select the weight functions  $w$  in practice. The following conjecture is inspired by the structure of the pointwise conditioning formula (1), and its use is illustrated in the two following examples, as well as for constructing fixed-state cGRFs over triangular or disk-shaped domains as described in the supplement.

**Conjecture 1** *Consider the set of linear boundary constraints  $\mathcal{L}_i u^A(x) = g_i(x)$  over  $x \in A_i$  for  $i = 1, \dots, n$ . For a given choice of projection functions  $f_1, \dots, f_n$  corresponding to*

boundary segments  $A_1, \dots, A_n$ , consider the vector of weight functions

$$w(x) = v^\top(x)M^{-1}(x), \quad (6)$$

where  $v : \mathcal{D} \rightarrow \mathbb{R}^n$  and  $M : \mathcal{D} \rightarrow \mathbb{R}^{n \times n}$  are functions with elements  $v_i(x) = k_0 \mathcal{L}_i^*(x, f_i(x))$  and  $M_{ij}(x) = \mathcal{L}_i k_0 \mathcal{L}_j^*(f_i(x), f_j(x))$ , respectively, for  $i, j = 1, \dots, n$ . Then, the cGRF representation (5) from Theorem 1 enforces the desired boundary constraints as long as conditions (3) and (4) are satisfied.

As an example, when  $\mathcal{D} = [0, T]$ ,  $\mathcal{L} = \{\mathcal{J}, \mathcal{J}\}$ ,  $g = \{\xi, \theta\}$ , and  $A = \{0, T\}$ , the cGRF representation based on this choice of  $w$  is equivalent to the Gaussian bridge representation.

Notice that as compared to the choices of  $w$  in Section 3.1.2, the recipe we propose here supports a more systematic way of constructing different types of cGRFs, at the expense of being more complicated. The optimal structure of  $w$  should be decided case by case. The following examples enforce mixed boundary constraints based on this choice of  $w$ .

**Example 4** Consider the unit square domain  $\mathcal{D} = [0, 1]^2$ , and the mixed boundary constraints  $\mathcal{L}_i u^{\{A_1, A_2\}}(x) = 0$  over  $x \in A_i$ , for  $i = 1, 2$ , where  $\mathcal{L}_i = a_i \partial_{x_1} + b_i$  with  $a_i, b_i \in \mathbb{R}$ ,  $A_1 = \{x \in \partial\mathcal{D} \mid x_1 = 0\}$ , and  $A_2 = \{x \in \partial\mathcal{D} \mid x_1 = 1\}$ . Let  $f_1(x) = (0, x_2)$ , and  $f_2(x) = (1, x_2)$ . A cGRF satisfying the mixed boundary constraints is obtained using (6) with  $w(x) = v^\top(x)M^{-1}(x)$ , where  $v_i(x) = k_0 \mathcal{L}_i^*(x, f_i(x)) = a_i \partial_{x_1} k_0(x, f_i(x)) + b_i k_0(x, f_i(x))$ , and  $M_{ij}(x) = \mathcal{L}_i k_0 \mathcal{L}_j^*(f_i(x), f_j(x)) = a_i a_j \partial_{x_1} \partial_{x'_1} k_0(f_i(x), f_j(x)) + a_i b_j \partial_{x_1} k_0(f_i(x), f_j(x)) + a_j b_i \partial_{x'_1} k_0(f_i(x), f_j(x)) + b_i b_j k_0(f_i(x), f_j(x))$ , for  $i, j = 1, 2$ . Here  $\partial_{x_1}$  and  $\partial_{x'_1}$  differentiate  $k_0$  with respect to the first and second arguments, respectively. As special cases, when  $a_0 = a_1 = 0$ , the cGRF enforces fixed-state constraints. When  $b_0 = b_1 = 0$ , the cGRF enforces fixed-derivative constraints. The mixed boundary constraints here also include the one-sided constraints, when  $a_0 = b_0 = 0$  or  $a_1 = b_1 = 0$ . See Figure 5 and the left panel in

Figure 2 for cGRFs with mixed boundary constraints on 1- and 2-dimensional domains.

**Example 5** *Certain boundary constraints that fall outside the scope of Theorem 1 by violating condition (3) can be re-formulated to fit the cGRF framework. Suppose we want to enforce  $\partial_{x_1} u^A(x_1, x_2) = 0$  at  $A = \{(x_1, x_2) \in \partial\mathcal{D} \mid x_2 = 0\}$ , on  $\mathcal{D} = [0, 1]^2$ . Let  $f(x_1, x_2) = (x_1, 0)$ . Notice that  $\partial_{x_1} u \circ f(x_1, x_2) = \partial_{x_1} u(x_1, 0)$  is less smooth than  $u(x_1, x_2)$  in the  $x_1$  dimension, violating condition (3). Nevertheless, we can enforce this boundary constraint indirectly by translating it into  $u(x_1, x_2) = c$  at  $A$  for some constant  $c$ , if known. Condition (3) is satisfied for the corresponding cGRF  $u^A(x_1, x_2) = u(x_1, x_2) + w(x_1, x_2) (c - u \circ f(x_1, x_2))$ , where  $w(x_1, x_2) = k((x_1, x_2), (x_1, 0)) k((x_1, 0), (x_1, 0))^{-1}$  is obtained using equation (6). The application on tensile testing in Section 4 demonstrates the enforcement of this type of boundary constraint.*

## 4 Applications

We consider some illustrative applications where replacing an unconstrained with a constrained probability model improves predictive performance and leads to more physically realistic results. We discuss the application of cGRFs to probabilistic numerical methods, data-driven discovery of dynamic systems, and inference for a displacement field from limited experimental measurements to study a material's response to pulling forces. Since the temporal and spatial dimensions are often treated differently in applications, we will use the notation  $u^A(t, x)$  for cGRF models defined over a spatio-temporal domain.

### 4.1 Probabilistic solvers for PDE boundary value problems

Partial differential equations (PDEs) model states implicitly by relating them to their derivatives with respect to spatial or temporal variables. Inference requires an explicit representation of the state, or solution, which in many cases is only available numerically. The

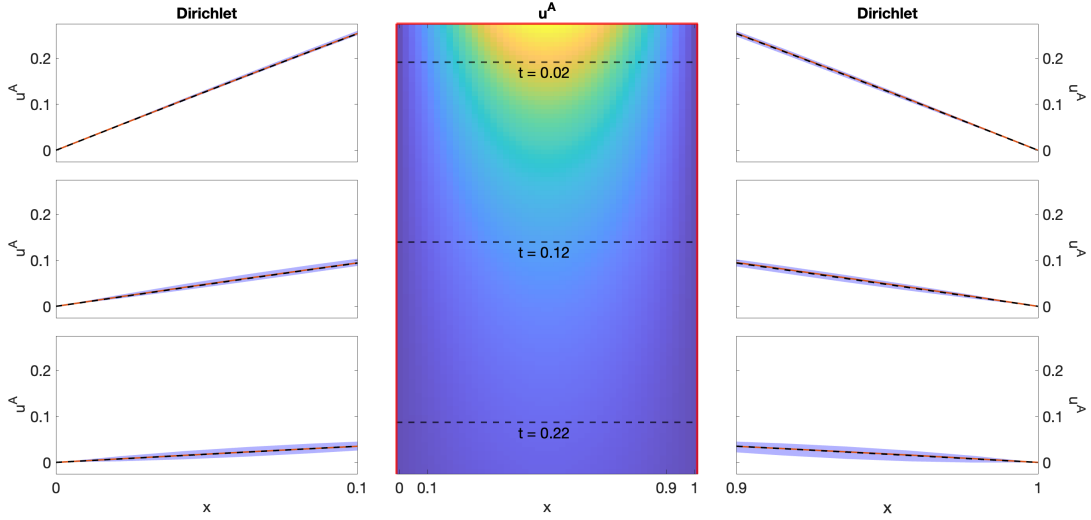


Figure 7: Center panel: mean probabilistic solution with initial condition  $u(t, x) = \sin(\pi x)$  and Dirichlet boundary conditions along red solid lines. Left and right panels: empirical estimates of posterior uncertainty near  $x = 0$  and  $x = 1$  for three time steps marked by dashed lines in the center panel. Posterior means are shown in orange, pointwise 95% credible intervals are represented by blue bands.

resulting unmodeled discretization uncertainty can lead to biased inference on calibration parameters, as well as over-confident uncertainty estimates. This has spurred recent interest in the field of probabilistic numerics (see [Cockayne et al. \(2019\)](#) for a comprehensive review) which seeks to model this type of uncertainty via so-called *probabilistic solvers* and propagate it through the statistical inverse problem. Careful modeling ensures that the resulting structured uncertainty agrees with the underlying dynamics. This requires choosing a prior over the state that reflects its known structure, including all boundary conditions. However, such priors were previously unavailable, and pointwise-conditioned GRFs were used, leading to the potential for numerical instability and less realistic modeling.

In one example, [Chkrebtii et al. \(2016\)](#) propose a state-space probabilistic solver which conditions a prior GRF model of the state on iterative evaluations of the PDE information operator. To illustrate the use of cGRFs in this setting, we consider the heat equation under two distinct sets of initial and boundary conditions over the temporal domain  $[0, 0.25]$  and the spatial domain  $[0, 1]$ . Let  $\mathcal{D} = [0, 0.25] \times [0, 1]$ , and let  $u : \mathcal{D} \rightarrow \mathbb{R}$  be the solution

satisfying the PDE  $u_t(t, x) = u_{xx}(t, x)$ ,  $(t, x) \in \mathcal{D}$ , with boundary constraints

$$\begin{aligned}\mathcal{L}_1 u(t, x) &= g_1(x), \quad (t, x) \in A_1, \\ \mathcal{L}_2 u(t, x) &= g_2(t), \quad (t, x) \in A_2, \\ \mathcal{L}_3 u(t, x) &= g_3(t), \quad (t, x) \in A_3,\end{aligned}\tag{7}$$

for linear operators  $\mathcal{L} = \{\mathcal{L}_1 = \mathcal{I}, \mathcal{L}_2, \mathcal{L}_3\}$  and target functions  $g = \{g_1, g_2, g_3\}$ , to be defined next for two distinct examples. The boundary segments are  $A = \{A_1, A_2, A_3\} = \{\{0\} \times [0, 1], (0, 0.25] \times \{0\}, (0, 0.25] \times \{1\}\}$ . Following [Chkrebtii et al. \(2016\)](#), we discretize the spatio-temporal domain by a  $100 \times 16$  uniform grid, and carry out a “forward in time, continuous in space” sampling strategy which sequentially updates the joint prior  $(u, u_t, u_{xx}) \sim cGRF(\mathcal{L}, g, A, m_0, k_0)$  on synthetic data about  $u_{xx}$  across the domain. We use a squared exponential base covariance  $k_0$  with length-scale hyperparameters 0.0175 in the temporal dimension and 0.4573 in the spatial dimension, proportional to the temporal and spatial step sizes, respectively. The prior precision hyperparameter is set to 1. The probabilistic solution is obtained by marginalizing over the synthetic data and concentrates on the exact solution  $u$  as the grid size grows.

Figures [7](#) and [8](#) visualize discretization uncertainty for the two examples relative to the solution approximated via a high-order adaptive numerical method (MATLAB `pdepe` solver; black dashed line) for two examples with different boundary constraints. The first example uses the initial condition  $u(t, x) = \sin(\pi x)$  and Dirichlet boundary conditions,  $g_2(t) = g_3(t) = 0$ , and  $\mathcal{L}_2 = \mathcal{L}_3 = \mathcal{I}$ . The second example uses the initial condition  $u(t, x) = \cos(\pi x) + 2$  and the mixed Robin and Neumann boundary conditions,  $g_2(t) = 3$ ,  $g_3(t) = 0$ , and  $\mathcal{L}_2 = \mathcal{I} + \partial_x$ ,  $\mathcal{L}_3 = \partial_x$ . The accumulation of discretization uncertainty is reflected in the widening of the credible intervals over time, while tending to zero as we approach the boundaries, reflecting the known physical mechanisms operating there.

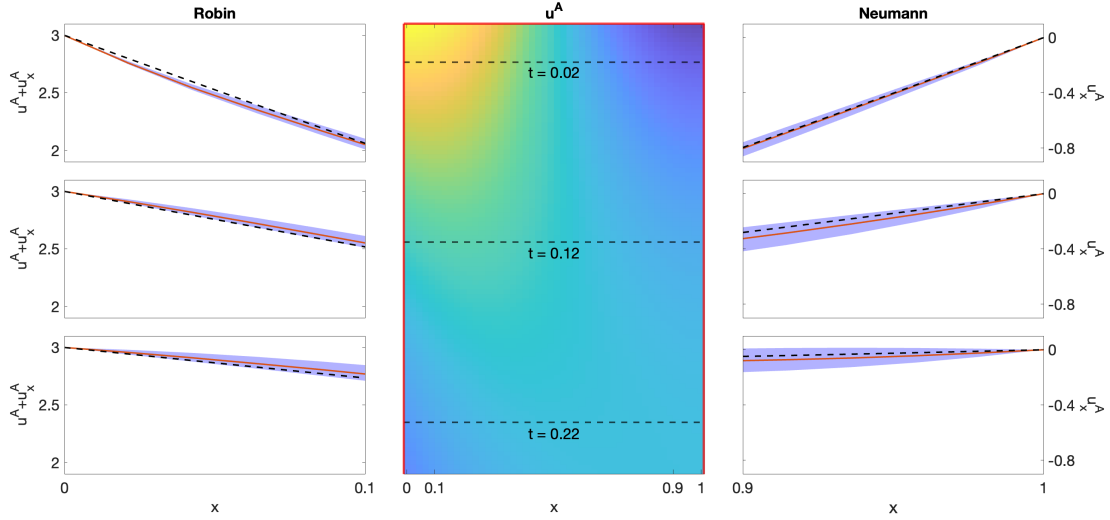


Figure 8: Center panel: mean probabilistic solution with initial condition  $u(t, x) = \cos(\pi x) + 2$  and mixed Robin and Neumann boundary conditions along red solid lines. Left and right panels: empirical estimates of posterior uncertainty near  $x = 0$  and  $x = 1$  for three time steps marked by dashed lines in the center panel. Posterior means are shown in orange, pointwise 95% credible intervals are represented by blue bands.

## 4.2 Data-driven discovery of dynamical systems

When a reliable mathematical model for the state is unavailable, a data-informed approach may be used for selecting an appropriate dynamical system from a set of candidates to help practitioners understand the physical phenomenon and predict its future behavior (e.g., [North et al. 2023, 2025](#)). For example, [Chen et al. \(2020\)](#) develop a GRF-assisted active learning algorithm that iteratively performs penalized linear regression of the temporal derivative on a collection of candidate model terms consisting of functions of the state and its spatial derivatives. These terms are evaluated at the input locations selected by an active learning algorithm. A GRF model of the latent state and its derivatives is used in the objective function to quantify the information gain from collecting data at potential input locations for choosing model components from a large set of candidates. Because GRFs do not in general enforce known boundary constraints, [Chen et al. \(2020\)](#) restricts attention to problems on unbounded domains. Introducing the known boundary constraints via cGRF modeling allows us to consider more realistic settings and can improve algorithm

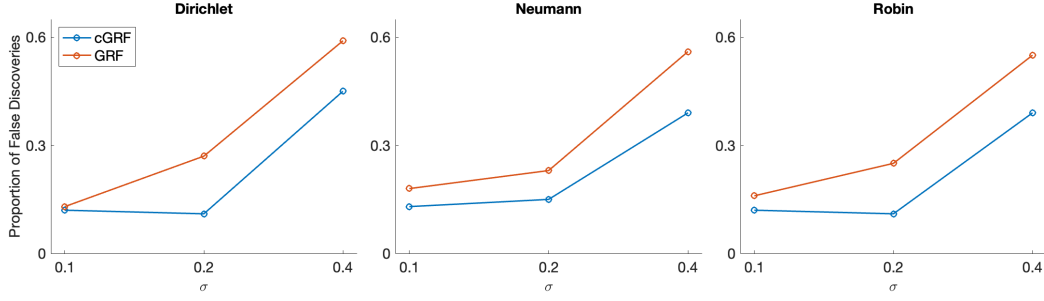


Figure 9: Proportion of false discoveries with cGRF (blue) and GRF (orange) at three levels of measurement error based on 100 simulations under different boundary constraints (left to right).

performance.

As an illustration, we apply this approach to learn Burger’s equation from simulated data under both a boundary-constrained cGRF model for the state and an unconstrained alternative. Consider the temporal domain  $[0, 1]$  and the spatial domain  $[-10, 10]$ . Let  $\mathcal{D} = [0, 1] \times [-10, 10]$ , and let  $u : \mathcal{D} \rightarrow \mathbb{R}$  be the underlying state satisfying the differential equation model  $u_t(t, x) = u_{xx}(t, x) - uu_x(t, x)$ ,  $(t, x) \in \mathcal{D}$  with boundary constraints in (7), for linear operators  $\mathcal{L} = \{\mathcal{L}_1 = \mathcal{I}, \mathcal{L}_2, \mathcal{L}_3\}$  and target functions  $g = \{g_1, g_2, g_3\}$ , to be defined later for three distinct examples. The boundary segments are  $A = \{A_1, A_2, A_3\} = \{\{0\} \times [-10, 10], (0, 1] \times \{-10\}, (0, 1] \times \{10\}\}$ . We use tri-modal initial condition as in [Chen et al. \(2020\)](#) corresponding to  $g_1(x) = 2 \exp(-15(x - 9)^2) + 1.5 \exp(-15(x + 1)^2) + \exp(-25(x + 9)^2)$ ,  $g_2(t) = \mathcal{L}_2 g_1(-10)$ , and  $g_3(t) = \mathcal{L}_3 g_1(10)$ . Algorithm performance is compared when using the unconstrained  $GRF(0, k_0)$  model and the constrained version,  $cGRF(\mathcal{L}, g, A, 0, k_0)$ . We test each setting under Dirichlet, Neumann, and Robin boundary conditions, corresponding to  $\mathcal{L}_2 = \mathcal{L}_3 = \mathcal{I}$ ,  $\mathcal{L}_2 = \mathcal{L}_3 = \partial_x$ , and  $\mathcal{L}_2 = \mathcal{L}_3 = \mathcal{I} + \partial_x$ , respectively. We adopt the algorithm settings in [Chen et al. \(2020\)](#), including using the squared exponential covariance  $k_0$ , the same collection of candidate terms  $\{1, u, u^2, u^3, u_x, \dots, u_x u_{xx}^2, uu_x u_{xx}\}$ , and levels of measurement error variance  $\sigma^2 = 0.2^2, 0.4^2$ . The two evaluation criteria are the proportion of false discoveries including



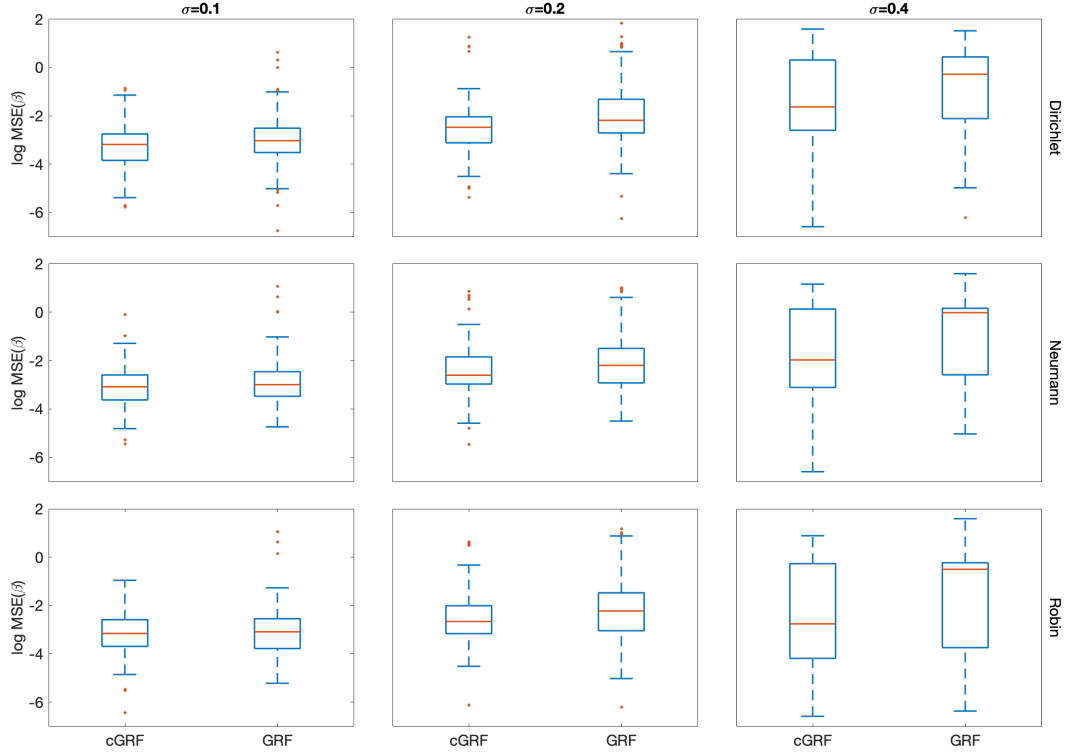


Figure 10: Log MSE for estimated coefficients based on 100 simulations using *cGRF* and *GRF* under different settings. Measurement standard deviations are  $\sigma = 0.1, 0.2$  and  $0.4$  from left to right. Boundary condition types are two-sided Dirichlet, Neumann and Robin from top to bottom.

missing the two correct terms and selecting the remaining false terms, and the log mean squared error (MSE) of the estimated coefficients. As shown in Figures 9 and 10, performance in both metrics is improved when using *cGRFs* by accounting for the additional information available at the boundary. The supplement also provides a frequency plot for falsely identified terms based on 100 simulations.

### 4.3 Boundary-constrained state estimation

Materials used in industrial applications are subjected to a variety of tensile forces. The tensile test is a fundamental experimental method in materials science engineering for measuring a material's response to these forces. During the test, discrete measurements of the displacement field are recorded as a dog-bone-shaped specimen is stretched upward by a

moving crosshead at a constant speed until fracture (see illustration in Figure 1). The strain field is then calculated as the spatial derivative of the displacement field along the vertical ( $x_2$ ) direction, and together with the stress measurements, is used to construct the stress–strain curve. This curve establishes critical material properties, including Young’s modulus, yield strength, ultimate tensile strength, and elongation at fracture, and its reliability depends on the accuracy of the displacement predictions at unobserved locations. In this section, we evaluate the predictive performance of GRF-based estimation of displacement from discrete measurements with and without prior boundary constraint enforcement. The data, shown in Figure 1, is obtained using the COMSOL software for multiphysics simulation.

Consider the temporal domain  $[0, 1]$  and the spatial domain  $\mathcal{D}_s$ , which is a dog-bone shaped spatial domain with lower boundary  $A_1 = \{(x_1, x_2) \mid x_2 = -10\}$  and upper boundary  $A_2 = \{(x_1, x_2) \mid x_2 = 10\}$ , marked in red in the left panel of Figure 1. Denote  $\mathcal{D} = [0, 1] \times \mathcal{D}_s$ , and  $A = \{A_1, A_2\}$ . Let  $u : \mathcal{D} \rightarrow \mathbb{R}$  be the displacement field in the vertical ( $x_2$ ) direction. Then the boundary constraints are  $u(t, x_1, x_2) = 0.005t$  at  $x_2 = 10$  and  $u(t, x_1, x_2) = 0$  at  $x_2 = -10$ , meaning the top of the specimen at  $A_2$  is pulled upwards by the moving crosshead at the constant speed 0.005 mm/s, while the bottom side is held in place and remains stationary. Notice that no constraints are necessary on the displacement field along the vertical sides of the domain (segments not highlighted in red in the first panel of Figure 1). Notice also that although the specimen is stretched, the spatial domain remains unchanged, because displacement is measured relative to the starting locations.

Let  $y_i = u(t_i, x_i) + \epsilon_i$ ,  $i = 1, \dots, N$  be noisy measurements of displacement with  $\epsilon_i \stackrel{ind}{\sim} N(0, \sigma^2)$ . We consider two prior models for  $u$ : an unconstrained GRF with 0 mean and squared exponential covariance  $k_0$ , and a cGRF constructed from a base GRF with the same mean and covariance, i.e.,  $cGRF(\mathcal{L}, g, A, 0, k_0)$  with  $\mathcal{L} = \{\mathcal{J}, \mathcal{J}\}$ , and  $g = \{0, 0.005t\}$ .

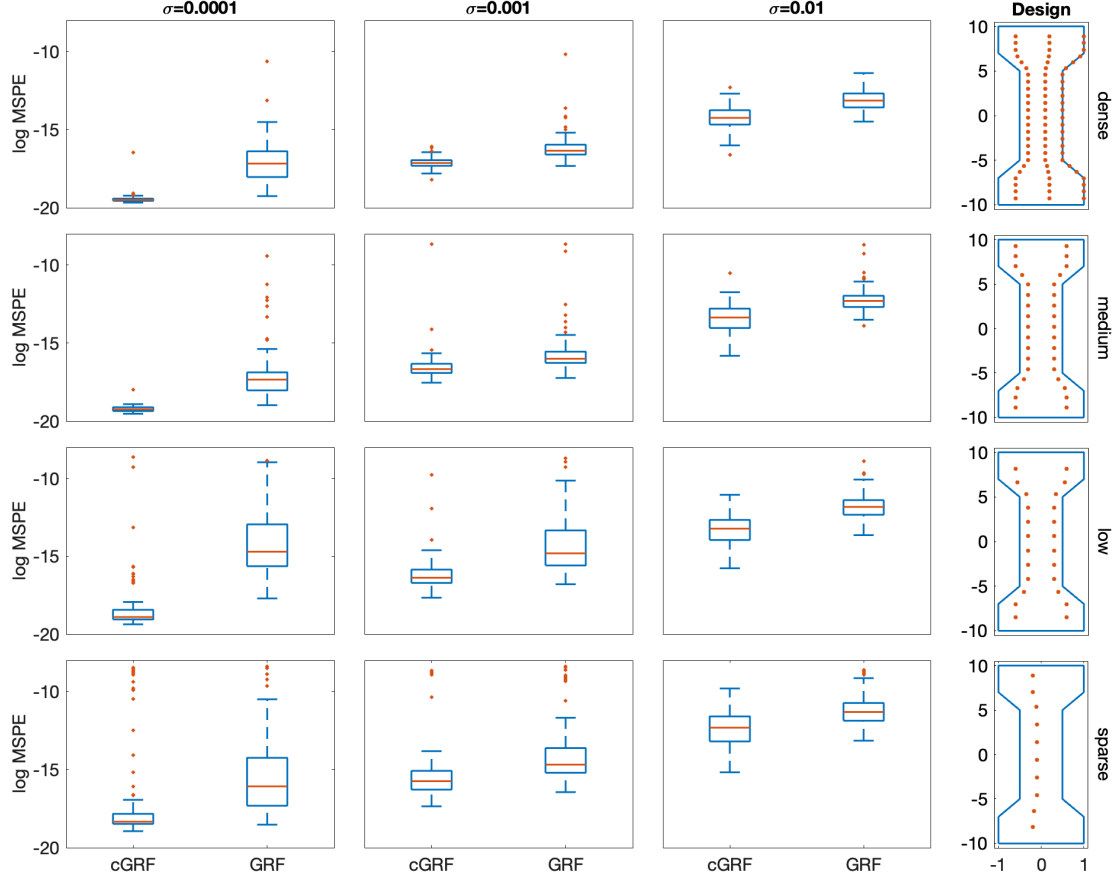


Figure 11: Box plots of log MSPE for displacement based on 100 simulations comparing the effect of constrained and unconstrained GRF priors under different settings. Measurement error standard deviations are  $\sigma = 0.0001, 0.001$  and  $0.01$  from left to right. Designs are dense, medium, low and sparse from top to bottom. The right column shows the measurement spatial locations.

The dataset is split into training, validation and testing data, at times  $t \in \{0, 0.3, 0.6, 0.9\}$ ,  $t \in \{0.1, 0.4, 0.7, 1\}$  and  $t \in \{0.2, 0.5, 0.8\}$ , respectively. Discrete measurements in the spatial domain are collected according to four designs shown in the right column of Figure 11. We select optimal hyperparameters for both the *cGRF* and its unconstrained counterpart by minimizing mean square prediction error (MSPE) based on the validation data. Predictive performance is evaluated at the test locations via the MSPE under four different designs and three different noise levels. As shown in Figure 11, boundary-constrained state estimation via *cGRF* outperforms the unconstrained case in all scenarios. Notice that outliers with large log MSPE, represented by orange dots in Figure 11, typically oc-

cur when the numerical optimizer for hyperparameter tuning converges to local minima, corresponding to small values of length-scale in the  $x_2$  dimension.

## 5 Conclusion

An important challenge in working with Gaussian random field models in physical, environmental, and engineering applications is the difficulty of directly enforcing linear boundary constraints on the states, while retaining their modeling and computational advantages. We developed a novel framework to construct constrained GRFs over multi-dimensional, convex domains by transforming so-called base GRFs, and inheriting their smoothness properties. Importantly, our definition of a boundary-constrained process does not require establishing the existence of conditioned measures to constrain states over continuous boundaries. We showcased the new cGRF model in a variety of applications where boundary constraints add important physics-based information to the inference procedure and lead to performance improvement over their unconstrained counterparts. Applications of this framework are wide-ranging and include any problem in which the user has prior knowledge about the state’s behavior at the boundaries.

Our case study highlights the potential for impact of this method in material science engineering where high fidelity reduced order models and simulation are an important growth area for the certification and qualification of additively manufactured components. We explored the example of tensile tests where one typically knows the displacements at the grips (e.g., a fixed lower grip and a prescribed upward motion at the upper grip) in advance. Incorporating these fixed boundary conditions into a cGRF-based inference framework ensures that the predicted displacement field exactly satisfies the physical constraints at the specimen ends, resulting in more accurate full-field predictions and more realistic uncertainty quantification. This improved inference propagates directly to the stress-strain

curve and the estimation of material properties, such as Young’s modulus and failure strain, which depend sensitively on the accuracy of the strain measurements derived from the displacement field. Such enhancements are particularly crucial for additive manufacturing processes, where materials often exhibit anisotropic, process-dependent mechanical behavior (Cai et al. 2025). By capturing the true mechanical response with higher fidelity, the cGRF approach supports the qualification of additively manufactured parts for demanding, high-performance applications while potentially reducing the extent of destructive testing needed for validation.

Other modeling extensions include using cGRFs with fixed-state boundary constraints as local models for domain partitions to ensure state continuity. By partitioning the domain into regions each modeled by a stationary GRF, Gramacy & Lee (2008), Gramacy & Appleby (2015) and Huang et al. (2025) model global nonstationarity in the data, and enable distributed-memory computation in today’s high-performance-computing environments. A drawback is that this induces discontinuities in the underlying smooth states. In such cases, cGRF priors may be joined at the boundaries to enforce state continuity, yielding more physically realistic models. Moreover, extensions to enforce state differentiability at the partition joints are possible with cGRFs constrained on linear combinations of the state and its derivatives. Second, Bayesian data-driven discovery of dynamical systems is an important open area (North et al. 2025), and cGRF models of system states enable GRF-assisted algorithms (Chen et al. 2020). Finally, while the examples in our paper focus on 1-dimensional outputs, the cGRF framework naturally generalizes to multi-dimensional outputs. Different choices of projection and weight functions, as well as the potential to relax of the convexity assumption on the input domains are also worth further investigation and have the potential to broaden the applicability and flexibility of the approach. In general, the use of prior cGRF models to enforce continuous constraints on states leads to

further progress towards more realistic physics-informed uncertainty quantification.

## 6 Disclosure statement

No conflicts of interest exist, to the best of our knowledge.

## 7 Data Availability Statement

All data used in this manuscript was simulated.

## References

- Arfken, G. B., Weber, H. J. & Harris, F. E. (2012), *Mathematical Methods for Physicists: A Comprehensive Guide*, Academic Press.
- Banerjee, S., Carlin, B. P. & Gelfand, A. E. (2004), *Hierarchical Modeling and Analysis for Spatial Data*, Chapman and Hall/CRC.
- Bird, R. B., Stewart, W. E. & Lightfoot, E. N. (2006), ‘Transport phenomena’.
- Cai, Z., Yang, Z., Meng, L., Lin, K., Hou, Y., Sapanathan, T., Zhu, J. & Zhang, W. (2025), ‘Characterization of anisotropy in additively manufactured materials through instrumented indentation testing’, *Chinese Journal of Mechanical Engineering* **38**.
- Chen, J., Kang, L. & Lin, G. (2020), ‘Gaussian process assisted active learning of physical laws’, *Technometrics* **63**(3), 329–342.
- Chkrebtii, O. (2013), Probabilistic Solution of Differential Equations for Bayesian Uncertainty Quantification and Inference, PhD thesis, Simon Fraser University.

- Chkrebtii, O., Campbell, D., Girolami, M. & Calderhead, B. (2016), ‘Bayesian solution uncertainty quantification for differential equations’, *Bayesian Analysis* **11**.
- Cockayne, J., Oates, C. J., Sullivan, T. J. & Girolami, M. (2019), ‘Bayesian probabilistic numerical methods’, *SIAM Review* **61**(4), 756–789.
- Dalton, D., Lazarus, A., Gao, H. & Husmeier, D. (2024), ‘Boundary constrained gaussian processes for robust physics-informed machine learning of linear partial differential equations’, *Journal of Machine Learning Research* **25**(272), 1–61.  
**URL:** <http://jmlr.org/papers/v25/23-1508.html>
- Ding, L., Mak, S. & Wu, C. F. J. (2019), ‘Bdrygp: a new Gaussian process model for incorporating boundary information’, *arXiv: Methodology*.
- Gasbarra, D., Sottinen, T. & Valkeila, E. (2007), Gaussian bridges, in ‘Stochastic Analysis and Applications: The Abel Symposium 2005’, Springer, pp. 361–382.
- Gramacy, R. B. & Apley, D. W. (2015), ‘Local Gaussian process approximation for large computer experiments’, *Journal of Computational and Graphical Statistics* **24**(2), 561–578.
- Gramacy, R. B. & Lee, H. K. H. (2008), ‘Bayesian treed Gaussian process models with an application to computer modeling’, *Journal of the American Statistical Association* **103**(483), 1119–1130.
- Gulian, M., Frankel, A. & Swiler, L. (2022), ‘Gaussian process regression constrained by boundary value problems’, *Computer Methods in Applied Mechanics and Engineering* **388**, 114–117.
- Hahn, D. W. & Özisik, M. N. (2012), *Heat Conduction*, John Wiley & Sons, Ltd.
- Hosford, W. F. (2005), *Mechanical Behavior of Materials*, Cambridge University Press.

- Huang, H., Blake, L. R., Katzfuss, M. & Hammerling, D. M. (2025), ‘Nonstationary spatial modeling of massive global satellite data’, *Journal of Computational and Graphical Statistics* **0**(0), 1–14.
- North, J. S., Wikle, C. K. & Schliep, E. M. (2023), ‘A review of data-driven discovery for dynamic systems’, *International Statistical Review* **91**(3), 464–492.
- North, J. S., Wikle, C. K. & Schliep, E. M. (2025), ‘A Bayesian approach for spatio-temporal data-driven dynamic equation discovery’, *Bayesian Analysis* **20**(2), 375–404.
- Paciorek, C. J. (2003), Nonstationary Gaussian Processes for Regression and Spatial Modelling, PhD thesis, Carnegie Mellon University.
- Padilla-Segarra, A., Noble, P., Roustant, O. & Savin, E. (2025), ‘Physics-informed, boundary-constrained gaussian process regression for the reconstruction of fluid flow fields’.
- URL:** <https://arxiv.org/abs/2507.17582>
- Santner, T. J., Williams, B. J., Notz, W. I. & Williams, B. J. (2003), *The Design and Analysis of Computer Experiments*, Springer New York, NY.
- Schabenberger, O. & Gotway, C. A. (2004), *Statistical Methods for Spatial Data Analysis*, Chapman and Hall/CRC.
- Seeger, M. (2004), ‘Gaussian processes for machine learning’, *International Journal of Neural Systems* **14**(2), 69–106.
- Solin, A. & Kok, M. (2019), Know your boundaries: Constraining Gaussian processes by variational harmonic features, *in* ‘International Conference on Artificial Intelligence and Statistics’, pp. 2193–2202.



- Stein, M. L. (1999), *Interpolation of Spatial Data: Some Theory for Kriging*, Springer New York, NY.
- Stuart, A. M. (2010), ‘Inverse problems: A Bayesian perspective’, *Acta Numerica* **19**, 451–559.
- Tan, M. H. Y. (2018), ‘Gaussian process modeling with boundary information’, *Statistica Sinica* **28**(2), 621–648.
- Vernon, I., Jackson, S. E. & Cumming, J. A. (2019), ‘Known boundary emulation of complex computer models’, *SIAM/ASA Journal on Uncertainty Quantification* **7**(3), 838–876.
- Wang, J., Cockayne, J., Chkrebtii, O., Sullivan, T. J. & Oates, C. J. (2021), ‘Bayesian numerical methods for nonlinear partial differential equations’, *Statistics and Computing* **31**(55).
- Wang, X. & Berger, J. O. (2016), ‘Estimating shape constrained functions using Gaussian processes’, *SIAM/ASA Journal on Uncertainty Quantification* **4**(1), 1–25.
- Ye, W. & Tan, M. H. Y. (2022), ‘Multi-fidelity Gaussian process modeling with boundary information’, *Applied Stochastic Models in Business and Industry* **38**(2), 216–239.

# Supplement

## 1 Theoretical justifications

### 1.1 Proof of Theorem 1

Before proving Theorem 1, we expand Definition 1 to a random field  $u^A$  which is linearly constrained to satisfy *multiple* linear boundary constraints.

**Definition 2** For  $i = 1, \dots, n$ , let  $\mathcal{L}_i : \mathcal{H} \rightarrow \mathcal{H}'_i$  be a linear operator,  $g_i : \mathcal{D} \rightarrow \mathbb{R}$  be a target function,  $A_i \subset \partial\mathcal{D}$  be a segment of the boundary, and  $u^A : \mathcal{D} \times \Omega \rightarrow \mathbb{R}$  be a random field. We say  $u^A$  is linearly-constrained if for  $i = 1, \dots, n$ ,  $\mathcal{L}_i u^A$  is sample-continuous and  $\mathcal{L}_i u^A(x)$  equals  $g_i(x)$  for all  $x \in A_i$  almost surely.

The proof of Theorem 1 is as follows.

**Proof 1** For  $i = 1, \dots, n$  and  $x \in \mathcal{D}$ , with probability one,

$$\begin{aligned}\mathcal{L}_i u^A(x) &= \mathcal{L}_i u(x) + \sum_{j=1}^n \mathcal{L}_i [w_j(x)(g_j \circ f_j(x) - \mathcal{L}_j u \circ f_j(x))] \\ &= \mathcal{L}_i u(x) + g_i \circ f_i(x) - \mathcal{L}_i u \circ f_i(x),\end{aligned}$$

where the second equality follows from condition (4) of Theorem 1. Next, to show that  $\mathcal{L}_i u^A$  is sample-continuous, note that  $\mathcal{L}_i u \in \mathcal{H}'_i$  and  $g_i \circ f_i - \mathcal{L}_i u \circ f_i \in \mathcal{H}'_i$  imply that  $\mathcal{L}_i u^A \in \mathcal{H}'_i \subset \mathcal{C}(\mathcal{D})$ . Since for all  $x \in A_i$

$$\mathcal{L}_i u^A(x) = \mathcal{L}_i u(x) + g_i(x) - \mathcal{L}_i u(x) = g_i(x),$$

almost surely,  $u^A$  is linearly-constrained by Definition 2. Furthermore, since  $u^A$  is a linear transformation of a GRF, then it is also a GRF.

## 1.2 Relationship with existing methods

In Example 1, we construct cGRFs on the interval  $\mathcal{D} = [0, 1]$ . We first consider enforcing fixed-state constraint  $u(x) = 0$  at  $x = 0$ . Two such cGRFs are  $u^{\{0\}}(x) = u(x) - u(0)$  and  $u^{\{0\}}(x) = u(x) - (k(x, 0)/k(0, 0))u(0)$ , corresponding to  $w(x) = 1$  and  $w(x) = k(x, 0)/k(0, 0)$ , respectively.

Assuming  $u$  is sample-differentiable, the first representation has the same covariance as the integral-based method in Chkrebtii (2013), Ye & Tan (2022), where

$$k^{\{0\}}(x, x') = \int_0^x \int_0^{x'} \partial_z \partial_{z'} k_0(z, z') dz dz' = k_0(x, x') - k_0(x, 0) - k_0(0, x') + k_0(0, 0).$$

Assuming  $u(1) = 0$ , the second representation is the Gaussian bridge in Proposition 1 of Gasbarra et al. (2007) with  $\xi = \theta = 0$  and  $T = 1$ .

We then consider enforcing fixed-derivative constraint  $\partial_x u(x) = 0$  at  $x = 0$ . A cGRF is  $u^{\{0\}}(x) = u(x) - x \partial_x u(0)$ , corresponding to  $w(x) = x$ . For this particular case, the cGRF is equivalent to Eq. (27) in Dalton et al. (2024) with  $a(x) = h(x) = \hat{u}_2(x) = 0$ , and  $w(x)$  in the cGRF is equal to  $\phi(x)\nabla\phi(x)$ , where  $\phi$  is the normalized ADF from Dalton et al. (2024).

## 2 Implementation details

### 2.1 Example: cGRF on a triangular domain

Consider enforcing the fixed-state boundary constraints along two segments of a unit triangular domain  $\mathcal{D} = \{(x_1, x_2) \in \mathbb{R}^2 \mid x_1, x_2 \geq 0, x_1 + x_2 \leq 1\}$  with boundary  $\partial\mathcal{D}$ , as shown in the top row of Figure 6. We wish to construct  $u^A \sim cGRF(\mathcal{L}, g, A, m_0, k_0)$ , where  $\mathcal{L} = \{\mathcal{I}, \mathcal{J}\}$ ,  $g = \{0, 0\}$ , and  $A = \{A_1 = \{x \in \partial\mathcal{D} \mid x_1 = 0\}, A_2 = \{x \in \partial\mathcal{D} \mid x_1 + x_2 = 1\}\}$ ,

and  $x = (x_1, x_2)$ .  $m_0$  and  $k_0$  are mean and covariance functions for a sample-continuous unconstrained GRF. For example, set  $m_0 = 0$  and  $k_0$  to be a squared exponential covariance. As discussed in the manuscript, the representation for such a cGRF is not unique, and here we demonstrate the use of the recipe for  $w$  in Section 3.3, and two projection functions,  $f_1(x) = (0, x_2)$  and  $f_2(x) = (1 - x_2, x_2)$ , following directions  $(-1, 0)$  and  $(1, 0)$ , respectively. For  $x \in \mathcal{D}$ ,  $w(x) = v(x)M^{-1}(x)$ , where

$$v(x) = \begin{bmatrix} k_0(x, (0, x_2)) & k_0(x, (1 - x_2, x_2)) \end{bmatrix},$$

$$M(x) = \begin{bmatrix} k_0((0, x_2), (0, x_2)) & k_0((0, x_2), (1 - x_2, x_2)) \\ k_0((1 - x_2, x_2), (0, x_2)) & k_0((1 - x_2, x_2), (1 - x_2, x_2)) \end{bmatrix}.$$

Therefore,  $w(x) = [w_1(x) \ w_2(x)]^\top$ , where

$$w_1(x) = \frac{k_0(x, (0, x_2))k_0((1 - x_2, x_2), (1 - x_2, x_2)) - k_0(x, (1 - x_2, x_2))k_0((1 - x_2, x_2), (0, x_2))}{k_0((0, x_2), (0, x_2))k_0((1 - x_2, x_2), (1 - x_2, x_2)) - k_0((0, x_2), (1 - x_2, x_2))^2},$$

$$w_2(x) = \frac{k_0(x, (1 - x_2, x_2))k_0((0, x_2), (0, x_2)) - k_0(x, (0, x_2))k_0((0, x_2), (1 - x_2, x_2))}{k_0((0, x_2), (0, x_2))k_0((1 - x_2, x_2), (1 - x_2, x_2)) - k_0((0, x_2), (1 - x_2, x_2))^2}.$$

Notice for all  $x \in A_1$ , i.e.,  $x = (0, x_2)$  for  $x_2 \in [0, 1]$ ,  $w_1(x) = 1$  and  $w_2(x) = 0$ . Similarly, for all  $x \in A_2$ , i.e.,  $x = (1 - x_2, x_2)$  for  $x_2 \in [0, 1]$ ,  $w_1(x) = 0$  and  $w_2(x) = 1$ . In other words, condition (4) is satisfied using these  $w$ . Based on Theorem 1,

$$u^A(x) = u(x) - w_1(x)u(0, x_2) - w_2(x)u(1 - x_2, x_2).$$

Based on Lemma 1,

$$m^A(x) = 0,$$

$$\begin{aligned} k^A(x, x') &= k_0(x, x') - w_1(x')k_0(x, (0, x'_2)) - w_2(x')k_0(x, (1 - x'_2, x'_2)) \\ &\quad - w_1(x)k_0((0, x_2), x') - w_2(x)k_0((1 - x_2, x_2), x') + w_1(x')w_1(x)k_0((0, x_2), (0, x'_2)) \\ &\quad + w_1(x')w_2(x)k_0((1 - x_2, x_2), (0, x'_2)) + w_2(x')w_1(x)k_0((0, x_2), (1 - x'_2, x'_2)) \\ &\quad + w_2(x')w_2(x)k_0((1 - x_2, x_2), (1 - x'_2, x'_2)). \end{aligned}$$

Other types of cGRFs can be constructed following a similar procedure. We also provide MATLAB code for all the cGRFs constructed in the manuscript.

## 2.2 Example: cGRF on disk-shaped domain

Similarly, Figure 2 shows samples from a cGRF  $u^{\partial\mathcal{D}}$  constrained to  $(x_1 + x_2)^2$  at the circular boundary  $\partial\mathcal{D}$  of the unit disk  $\mathcal{D} = \{x = (x_1, x_2) \in \mathbb{R}^2 \mid x_1^2 + x_2^2 \leq 1\}$ . The cGRF is

$$u^{\partial\mathcal{D}}(x) = u(x) - (1 - w(x)) u(-(1 - x_2^2)^{1/2}, x_2) - w(x) u((1 - x_2^2)^{1/2}, x_2) + (x_1 + x_2)^2,$$

where  $w(x) = (x_1 + (1 - x_2^2)^{1/2}) / (2(1 - x_2^2)^{1/2})$ . Mean and covariance functions for  $u^{\partial\mathcal{D}}$  are

$$\begin{aligned}
m^{\partial\mathcal{D}}(x) &= (x_1 + x_2)^2, \\
k^{\partial\mathcal{D}}(x, x') &= k_0(x, x') - (1 - w(x'))k_0(x, (-(1 - x_2'^2)^{1/2}, x_2')) - w(x')k_0(x, ((1 - x_2'^2)^{1/2}, x_2')) \\
&\quad - (1 - w(x))k_0((-(1 - x_2^2)^{1/2}, x_2), x') - w(x)k_0(((1 - x_2^2)^{1/2}, x_2), x') \\
&\quad + (1 - w(x'))(1 - w(x))k_0((-(1 - x_2^2)^{1/2}, x_2), (-(1 - x_2'^2)^{1/2}, x_2')) \\
&\quad + (1 - w(x'))w(x)k_0(((1 - x_2^2)^{1/2}, x_2), (-(1 - x_2'^2)^{1/2}, x_2')) \\
&\quad + w(x')(1 - w(x))k_0((-(1 - x_2^2)^{1/2}, x_2), ((1 - x_2'^2)^{1/2}, x_2')) \\
&\quad + w(x')w(x)k_0(((1 - x_2^2)^{1/2}, x_2), ((1 - x_2'^2)^{1/2}, x_2')).
\end{aligned}$$

### 2.3 Example: cGRF with product covariance structure

Consider a base GRF  $u$  on the unit square domain  $\mathcal{D} = [0, 1]^2$  with mean function 0 and covariance function

$$k_0(x, x') = k_1(x_1, x_1')k_2(x_2, x_2').$$

Like in the second row in Figure 6, we wish to enforce two-sided parallel boundary constraints on  $A = \{(x_1, x_2) \in \partial\mathcal{D} \mid x_2 = 0 \text{ or } x_2 = 1\}$ . The representation is  $u^A(x_1, x_2) = u(x_1, x_2) - (1 - x_2)u(x_1, 0) - x_2u(x_1, 1)$ , for  $(x_1, x_2) \in \mathcal{D}$ , with mean function  $m^A(x) = 0$

and covariance function

$$\begin{aligned}
k^A(x, x') &= k_0(x, x') - (1 - x'_2)k_0(x, (x'_1, 0)) - x'_2k_0(x, (x'_1, 1)) \\
&\quad - (1 - x_2)k_0((x_1, 0), x') - x_2k_0((x_1, 1), x') + (1 - x'_2)(1 - x_2)k_0((x_1, 0), (x'_1, 0)) \\
&\quad + (1 - x'_2)x_2k_0((x_1, 1), (x'_1, 0)) + x'_2(1 - x_2)k_0((x_1, 0), (x'_1, 1)) + x'_2x_2k_0((x_1, 1), (x'_1, 1)) \\
&= k_1(x_1, x'_1)[k_2(x_2, x'_2) - (1 - x'_2)k_2(x_2, 0) - x'_2k_2(x_2, 1) - (1 - x_2)k_2(0, x'_2) - x_2k_2(1, x'_2) \\
&\quad + (1 - x'_2)(1 - x_2)k_2(0, 0) + (1 - x'_2)x_2k_2(1, 0) + x'_2(1 - x_2)k_2(0, 1) + x'_2x_2k_2(1, 1)] \\
&=: k_1(x_1, x'_1)k_2^A(x_2, x'_2).
\end{aligned}$$

Note that  $k_2^A$  is the covariance of a cGRF on the domain  $[0, 1]$  with state constraints at both endpoints, and the product covariance structure is preserved after the transformation. To produce Figure 6, we set  $k_1$  to be the periodic covariance in dimension  $x_1$  and Matérn in  $x_2$ .

## 2.4 Additional application results

### 2.4.1 Data-driven discovery of dynamical systems

Figure 11 provides additional results comparing false discovery rates using cGRFs versus their unconstrained versions.

## References

- Chkrebtii, O. (2013), Probabilistic Solution of Differential Equations for Bayesian Uncertainty Quantification and Inference, PhD thesis, Simon Fraser University.
- Dalton, D., Lazarus, A., Gao, H. & Husmeier, D. (2024), ‘Boundary constrained gaussian processes for robust physics-informed machine learning of linear partial differential equa-

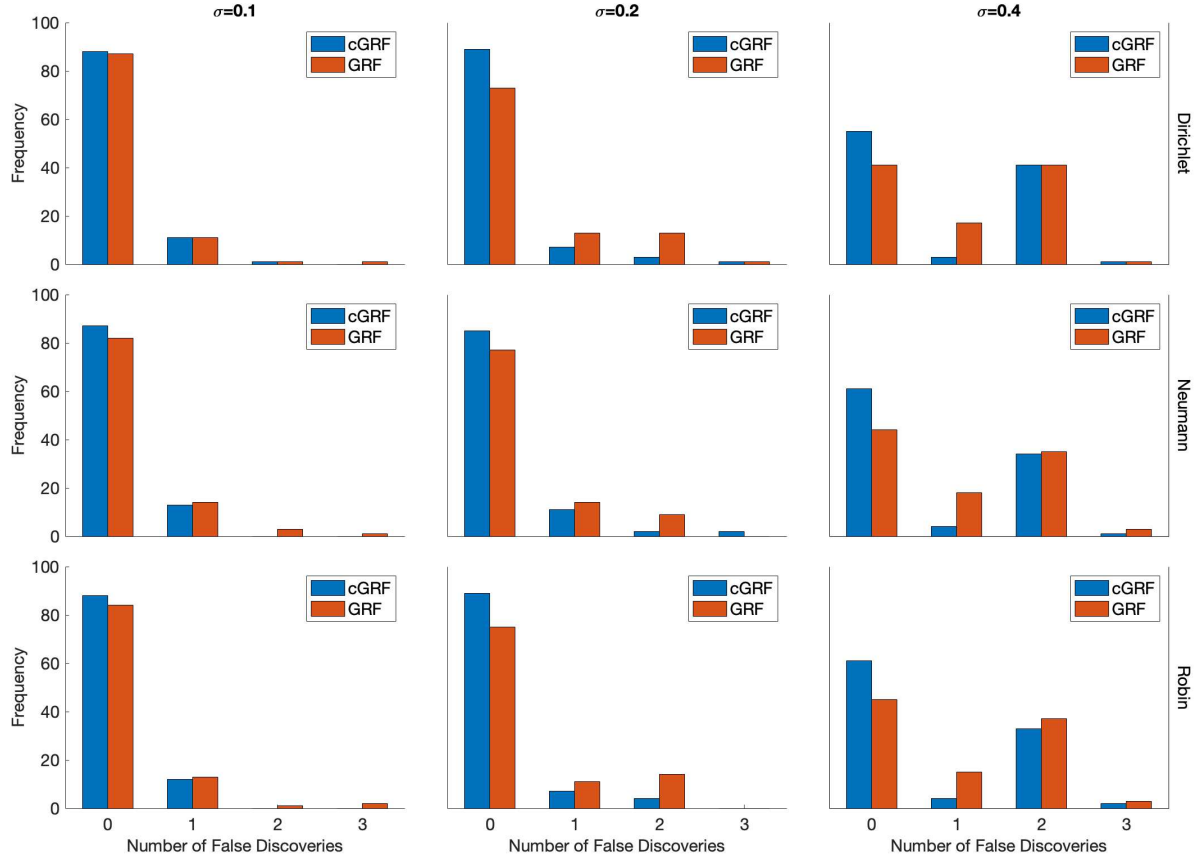


Figure 11: Frequencies of false discoveries in 100 simulations for  $cGRF$  in blue and  $GRF$  in orange, under different settings. Columns 1 – 3: measurement error  $\sigma = 0.1, 0.2$  and  $0.4$ , respectively. Rows 1 – 3: impose two-sided Dirichlet, Neumann and Robin boundary constraints, respectively.



tions’, *Journal of Machine Learning Research* **25**(272), 1–61.

**URL:** <http://jmlr.org/papers/v25/23-1508.html>

Gasbarra, D., Sottinen, T. & Valkeila, E. (2007), Gaussian bridges, *in* ‘Stochastic Analysis and Applications: The Abel Symposium 2005’, Springer, pp. 361–382.

Ye, W. & Tan, M. H. Y. (2022), ‘Multi-fidelity Gaussian process modeling with boundary information’, *Applied Stochastic Models in Business and Industry* **38**(2), 216–239.